Supplementary material

Construction of ultrafine ZnSe nanoparticles on/in amorphous carbon hollow nanospheres with high-power-density sodium storage

Shiyao Lu[a], Tianxiang Zhu[a], Hu Wu[a], Yuankun Wang[a], Jiao Li[a], Amr Abdelkader[b,c], Kai Xi[b,*], Wei Wang[b], Yanguang Li[d], Shujiang Ding[a], Guoxin Gao[a,*], and R. Vasant Kumar[b]

[a] Department of Applied Chemistry, School of Science, Xi'an Key Laboratory of Sustainable Energy Materials Chemistry, MOE Key Laboratory for Nonequilibrium Synthesis and Modulation of Condensed Matter, Xi'an Jiaotong University, Xi'an 710049, People's Republic of China

[b] Department of Materials Science and Metallurgy, University of Cambridge, Cambridge CB3 0FS, United Kingdom

[c] Department of Design and Engineering, Faculty of Science & Technology, Bournemouth University, Poole, Dorset, BH12 5BB, United Kingdom

[d] Institute of Functional Nano&Soft Materials (FUNSOM), Jiangsu Key Laboratory for Carbon-Based Functional Materials and Devices, Soochow University, Suzhou 215123, China

* Corresponding author.

E-mail addresses: gaoguoxin@mail.xjtu.edu.cn (G. X. Gao), kx210@cam.ac.uk (K. Xi)

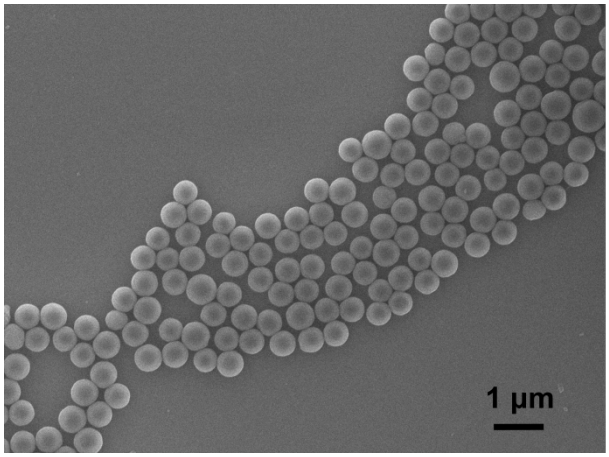

Figure S1. FESEM images of hollow polystyrene (PS) nanosphere templates.

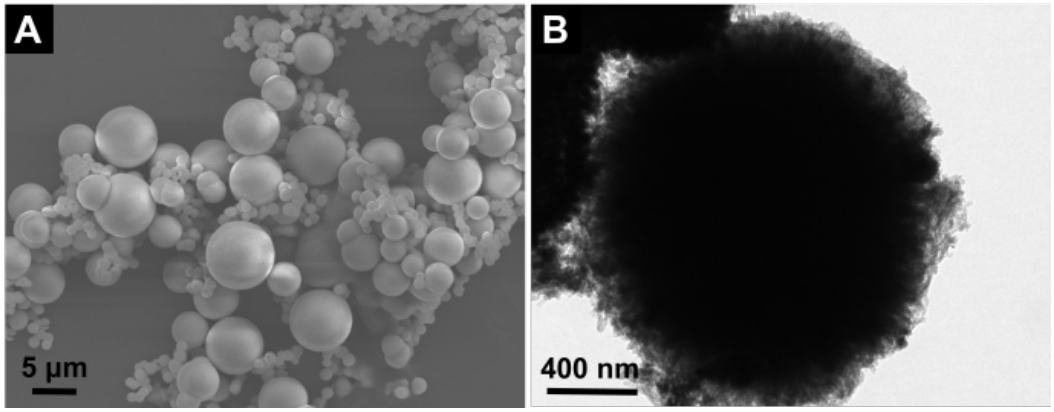

Figure S2. (A) FESEM and (B) TEM images of aggregated ZnSe MSs

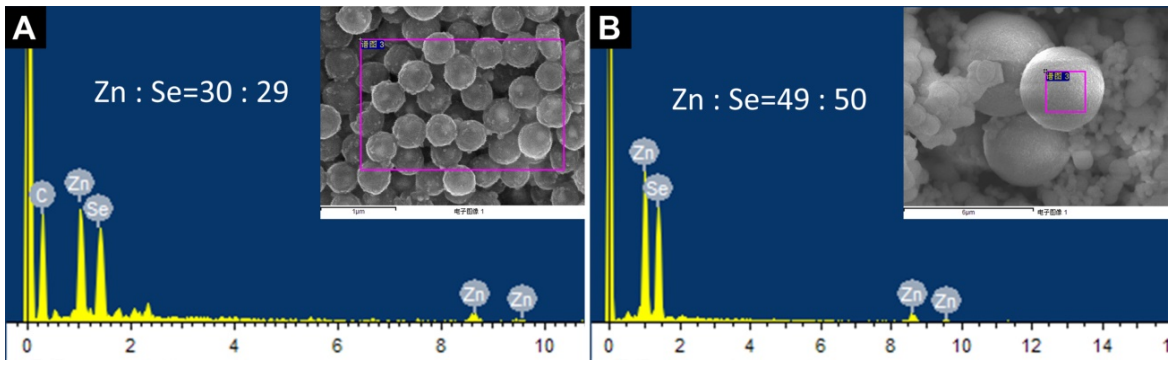

Figure S3. EDX patterns of (A) as-prepared ZnSe@HCNs and (B) ZnSe MSs.

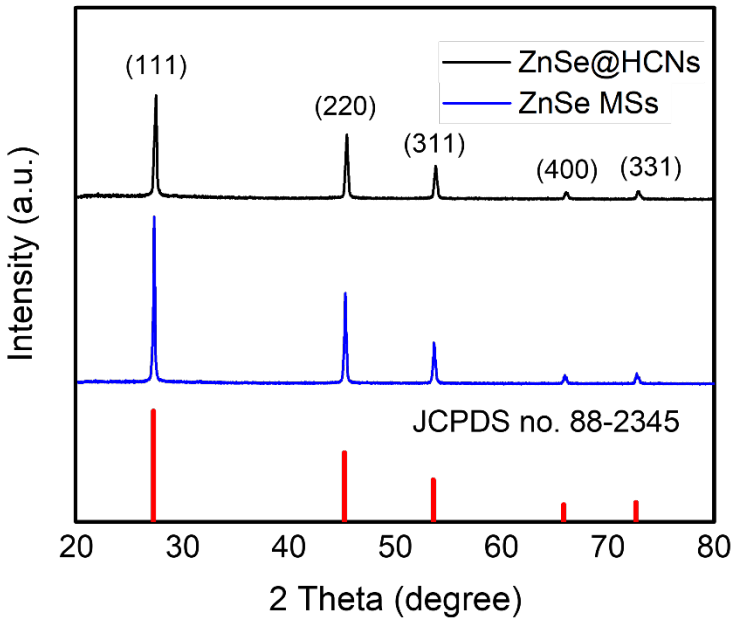

Figure S4. XRD patterns of as-prepared ZnSe@HCNs and aggregated ZnSe MSs

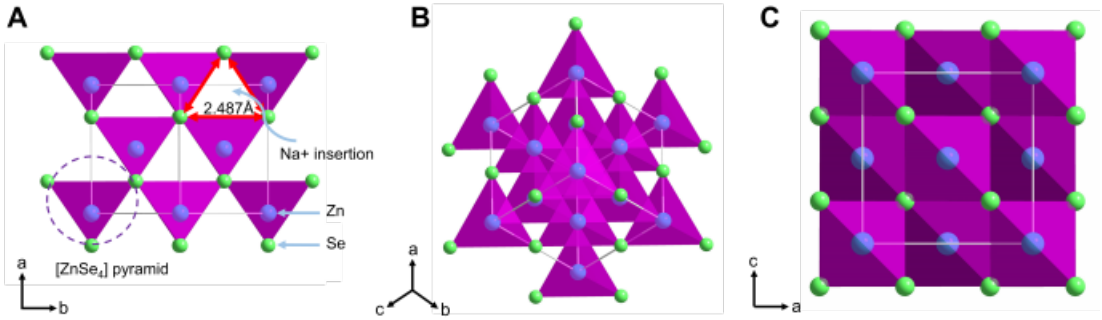

Figure S5. Crystal structures of ZnSe along different orientations: (A) [110]; (B) [111]; (C) [100].

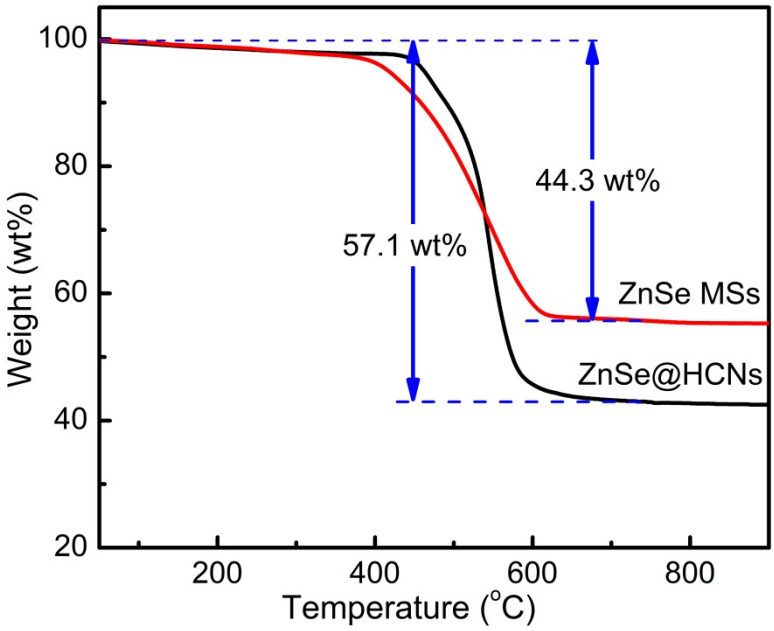

Figure S6. TGA curves of ZnSe@HCNs and ZnSe MSs at a heating ramp of 10 °C min^{-1}.

From TGA results, the main weight loss of the controlled sample is at about 382 °C, associated with the generation of the volatile SeO_2. The first thermal degradation event is taking place after 440 °C for the ZnSe@HCNs, indicating more thermal stability. This can be explained by the presence of some free Se in the controlled sample that decomposes faster than the alloyed nanoparticles in the ZnSe@HCNs. The mass content of ZnSe in the hybrid ZnSe@HCNs composites can be calculated by the equation: $m \times 57.1\% = mx \times 44.3\% + m \times (1 - x)$, where m represents the weight of ZnSe@HCNs composites and x refers to the percentage of pure ZnSe within the composites. Thus, the total carbon content is about 23.0 wt% in the final ZnSe@HCNs composites.

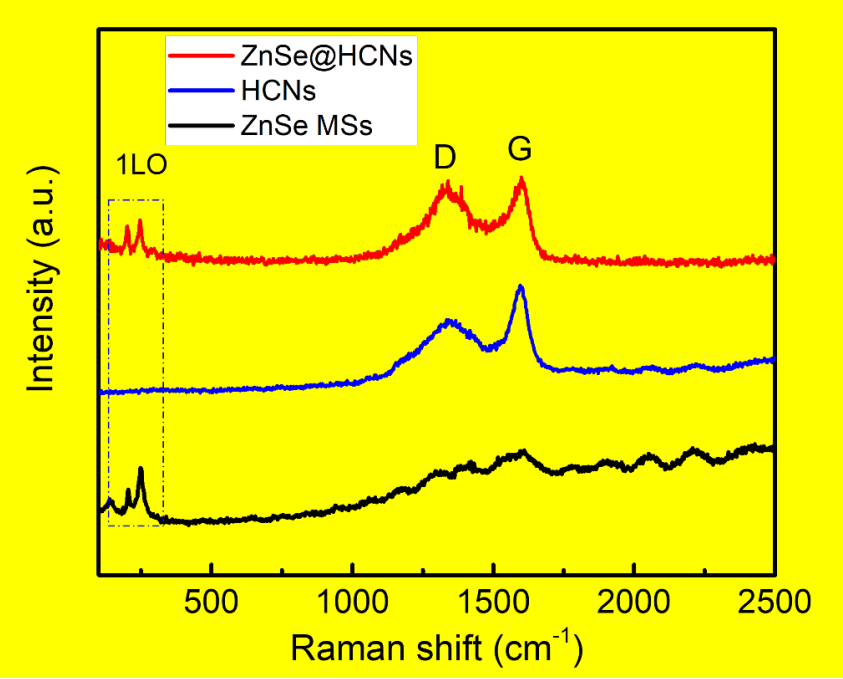

Figure S7. Raman spectra of as-prepared ZnSe@HCNs, aggregated ZnSe MSs and HCNs. Two characteristic peaks at 203.2 and 252.3 cm^{-1} exist on both samples, corresponding to the typical 1 LO modes of ZnSe.

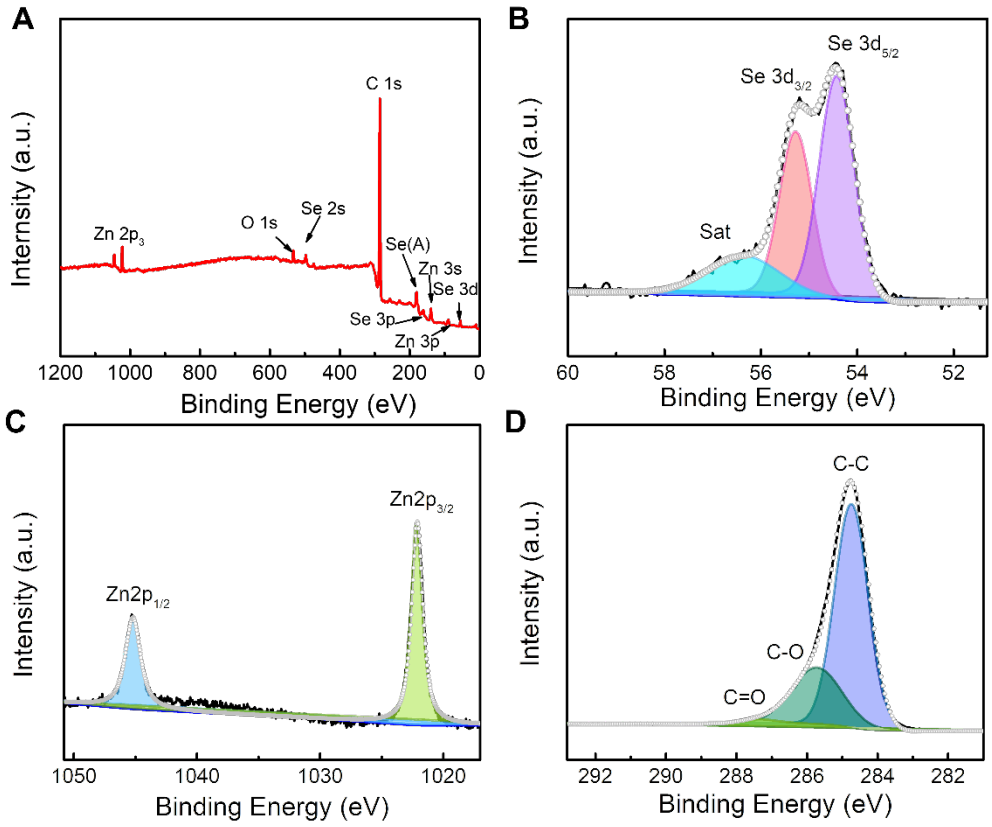

Figure S8. XPS spectra of as-prepared ZnSe@HCNs: (A) survey, (B) Se 2p, (C) Zn 2p, (D) C 1s.

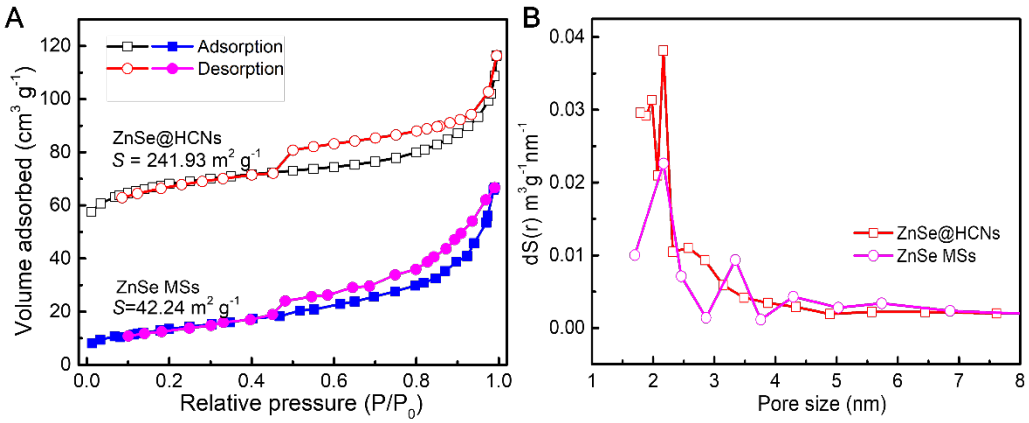

Figure S9. (A) N_2 adsorption-desorption isotherm and (B) pore size distributions of as-prepared ZnSe@HCNs and aggregated ZnSe MSs.

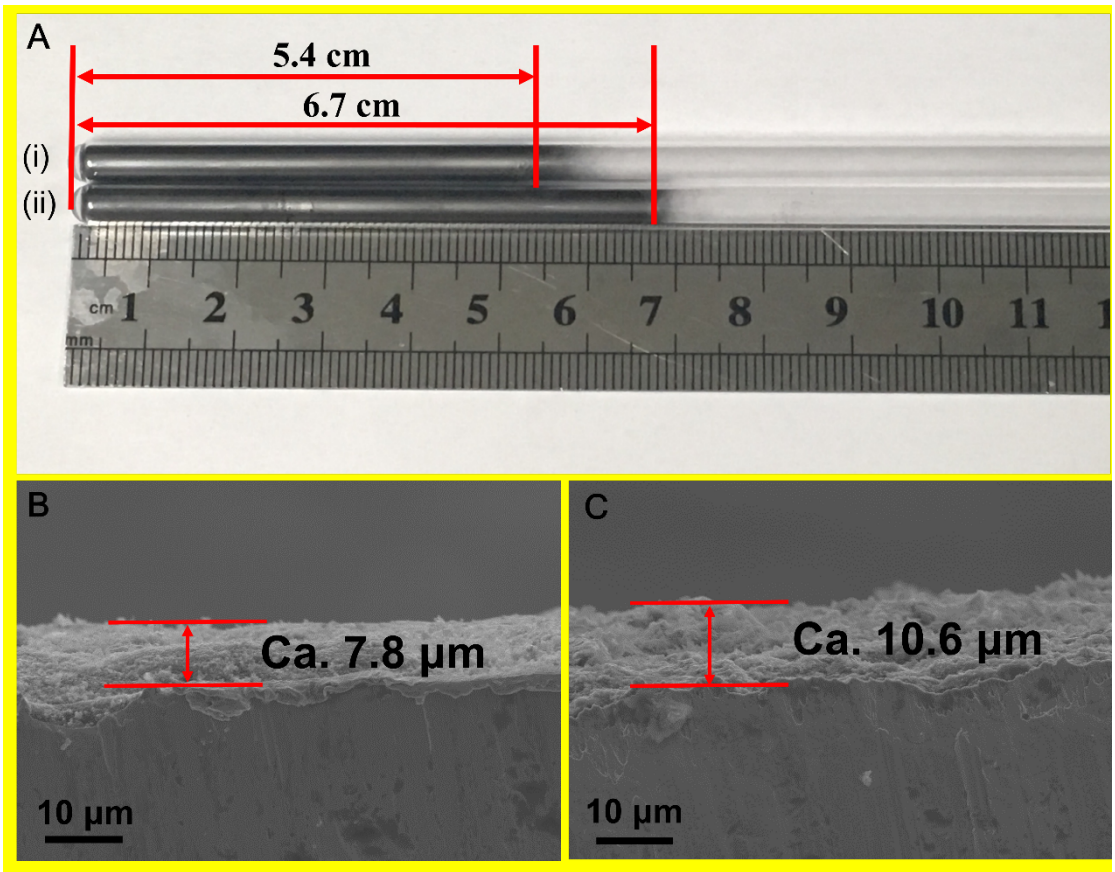

Figure S10 (A) Digital photograph of 0.4 g of (i) ZnSe@HCNs and (ii) HCNs tapped in quartz tubes with an inner diameter of *ca.* 4 mm, respectively. SEM images show the electrode thickness of the (B) ZnSe@HCNs (C) HCNs pasted on Cu foil.

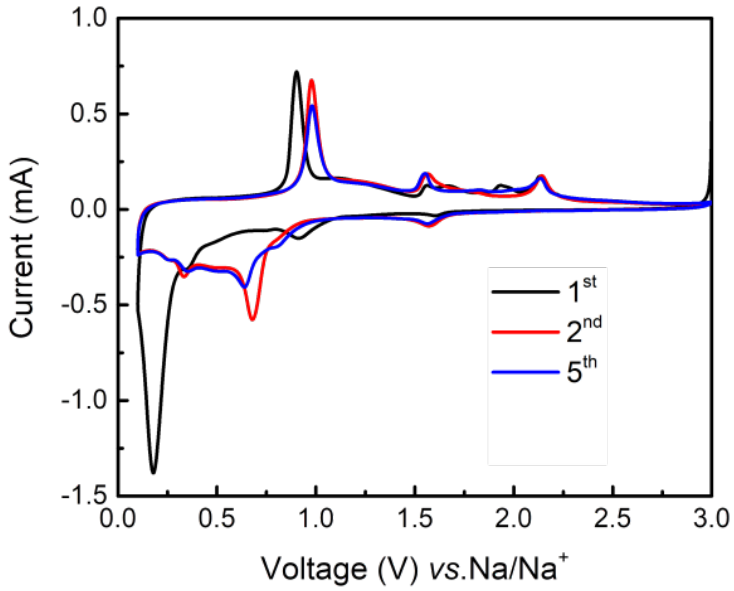

Figure S11. Initial CV curves of as-prepared ZnSe@HCNs at a scan rate of 0.5 mV s^{-1} in the voltage window between 0.1 and 3.0 V.

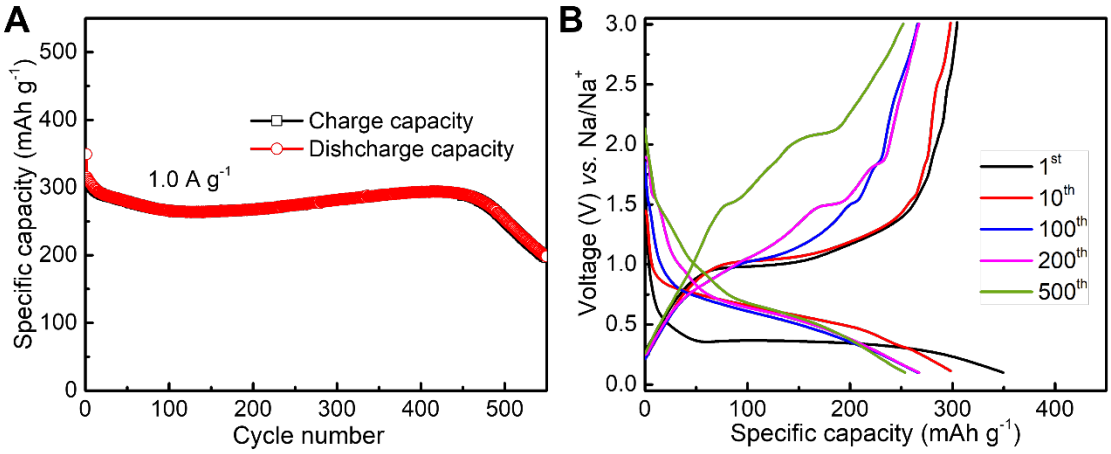

Figure S12. Electrochemical performance of aggregated ZnSe MSs anodes with 1.0 M $NaCF_3SO_3$ in DEGDME as electrolyte: (A) Cyclic stability, (B) Corresponding charge-discharge curves at 1.0 A g^{-1} in the cut-off voltage of 0.1-3.0 V.

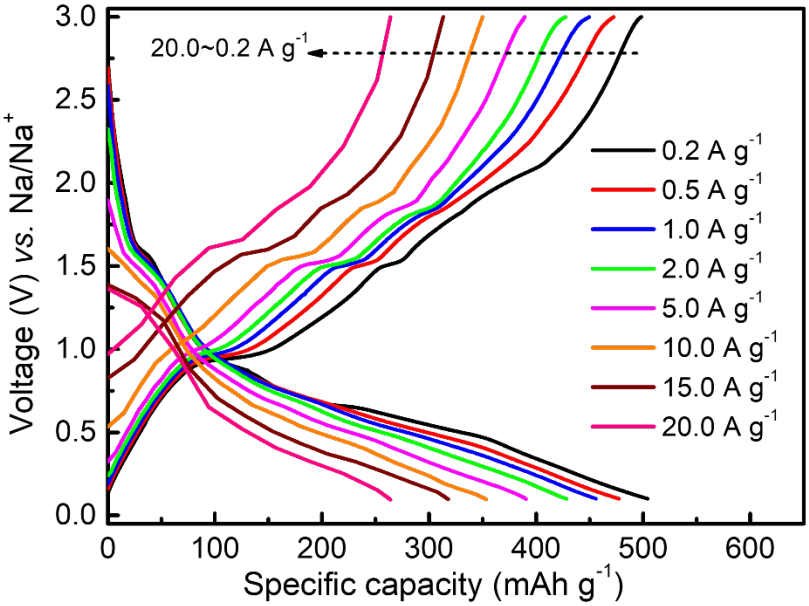

Figure S13. Charge-discharge curves of ZnSe@HCNs at various current densities ranging from 0.2 to 20.0 A g^{-1} between 0.1 and 3.0 V.

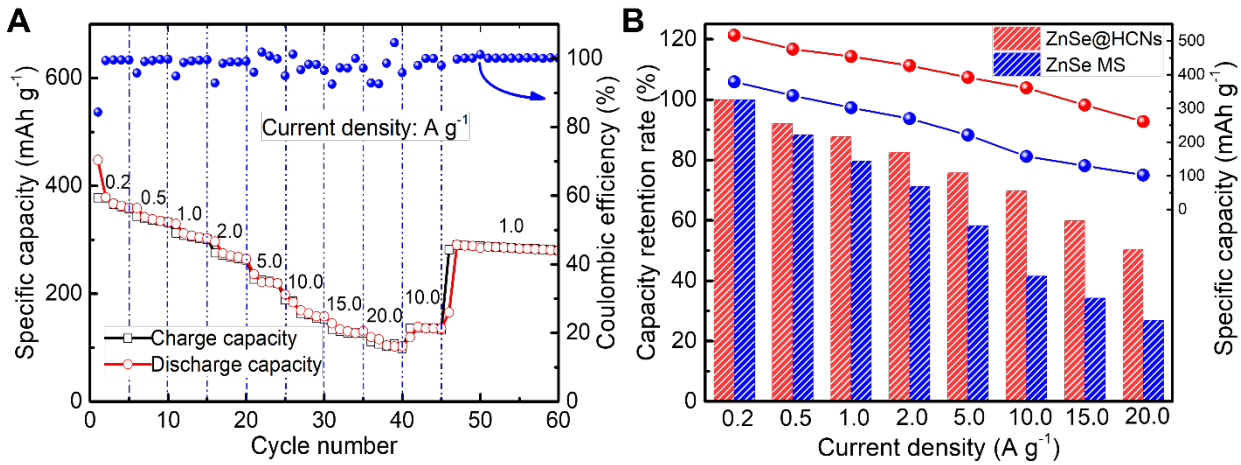

Figure S14. (A) Rate performance of aggregated ZnSe MSs anodes and (B) Capacity retentions of as-prepared ZnSe@HCNs and aggregated ZnSe MSs at various current densities ranging from 0.2 to 20.0 A g^{-1} between 0.1 and 3.0 V.

The capacity retentions of the ZnSe MSs samples dramatically drop to 26.9% with the current density increasing to 20.0 A g^{-1}, while the hybrid ZnSe@HCNs still give a high capacity retention of 53.6% with the 100-fold increase of current density.

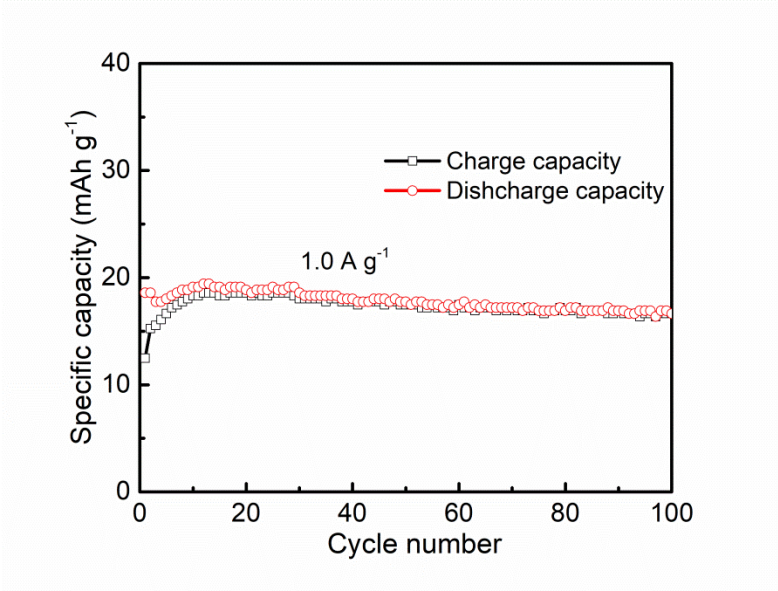

Figure S15. Cycle performance of pure HCNs at a current density of 1.0 A g^{-1} between 0.1 and 3.0 V.

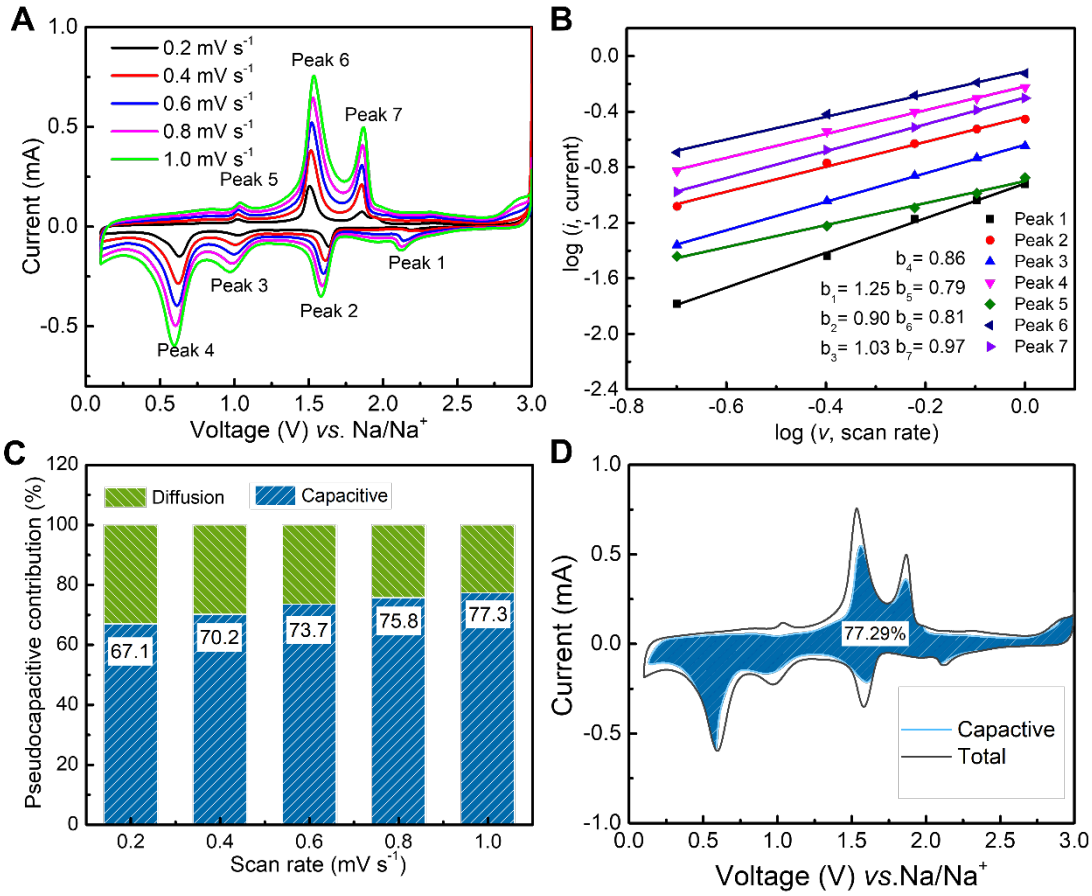

Figure S16. (A) CV curves of ZnSe MSs after 150 cycles at different scan rates; (B) corresponding log (*i*) versus log (*v*) plot at each redox peak; (C) percent of pseudocapacitive contribution at

different scan rates; (D) CV curve with pseudocapacitive fraction shown by blue region at a scan rate of 1 mV s^{-1}.

Briefly, the pseudocapacitive behaviors also exist for solid aggregated ZnSe MSs upon the electrochemical process, but the pseudocapacitive contributions of aggregated ZnSe MSs are much lower than those of hybrid ZnSe@HCNs, mainly due to the inadequate electrochemical reactions between Na^+ ions and solid ZnSe MSs

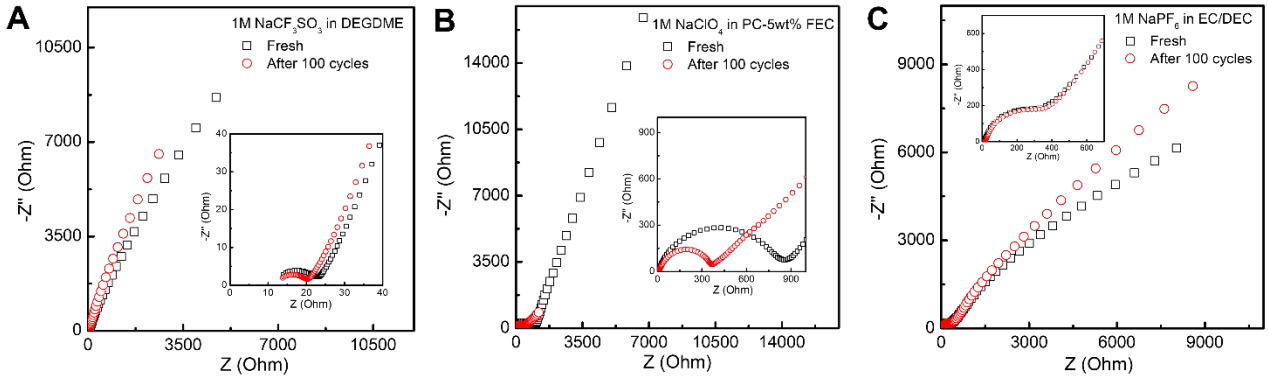

Figure S17. Nyquist plots of ZnSe@HCNs electrodes anodes in fresh and cycled cells using different electrolytes with an amplitude of 5.0 mV over the frequency range of 100 kHz and 0.01 Hz by applying a sine wave: (A) 1.0 M $NaCF_3SO_3$ in DEGDME; (B) 1.0 M $NaClO_4$ in PC with 5 wt% FEC; (C) 1.0 M $NaPF_6$ in EC/DEC (v/v = 1:1).

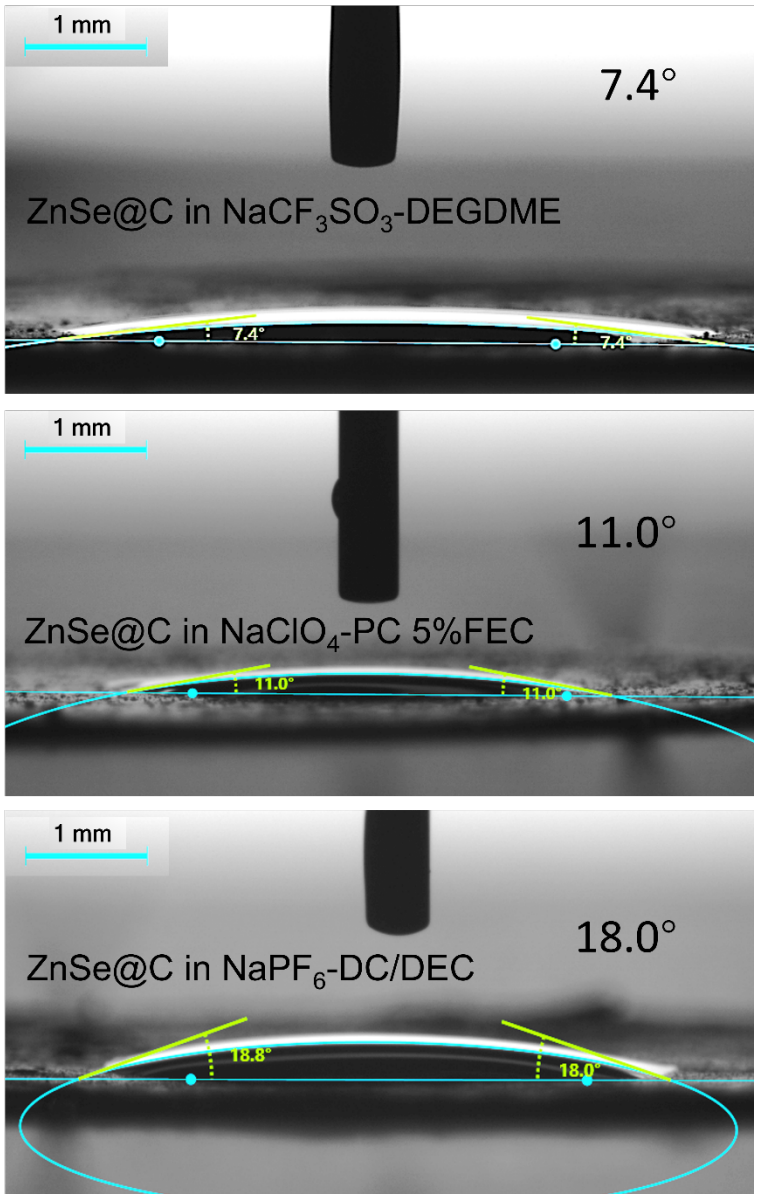

Figure S18. Contact angles measurements of different electrolytes on the ZnSe@HCNs electrodes: (A) 1.0 M $NaCF_3SO_3$ in DEGDME; (B) 1.0 M $NaClO_4$ in PC with 5 wt% FEC; (C) 1.0 M $NaPF_6$ in EC/DEC (v/v = 1:1).

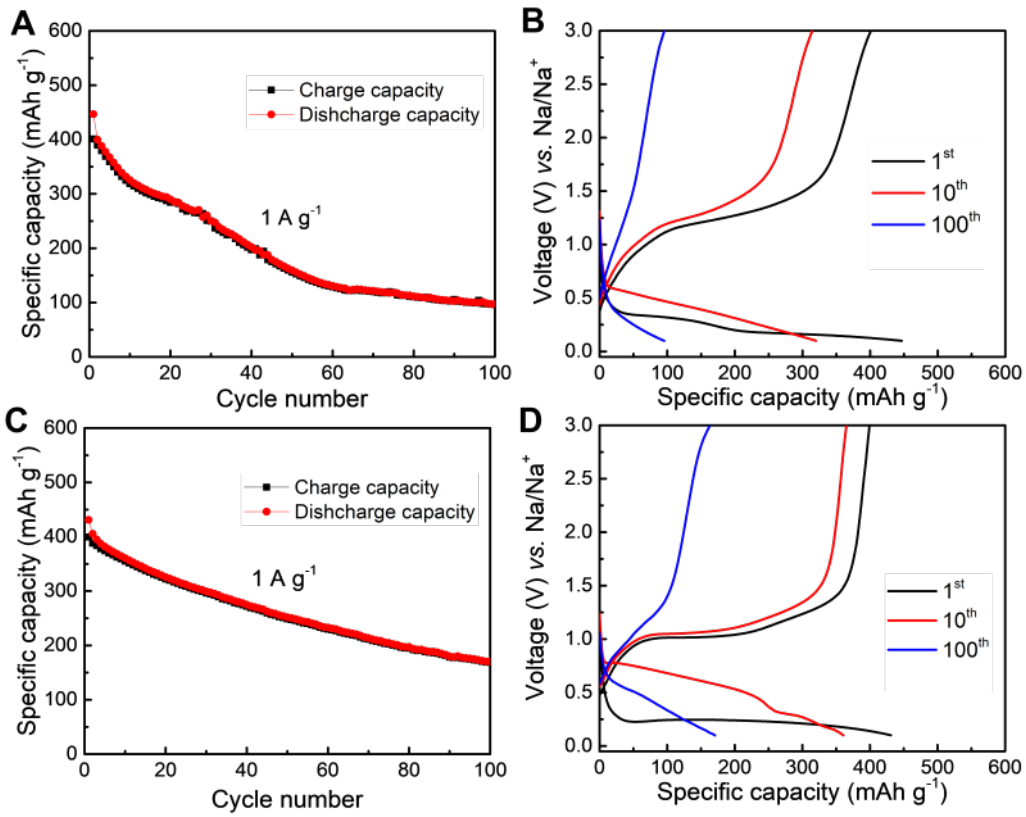

Figure S19. (A, C) Cycling performance and (B, D) Corresponding charge-discharge profiles of as-prepared ZnSe@HCNs at 1.0 A g^{-1}using different carbonate-based electrolytes: (A, B) 1.0 M $NaClO_4$ in PC with 5% FEC; (C, D) 1.0 M $NaPF_6$ in EC/DEC (v/v = 1:1).

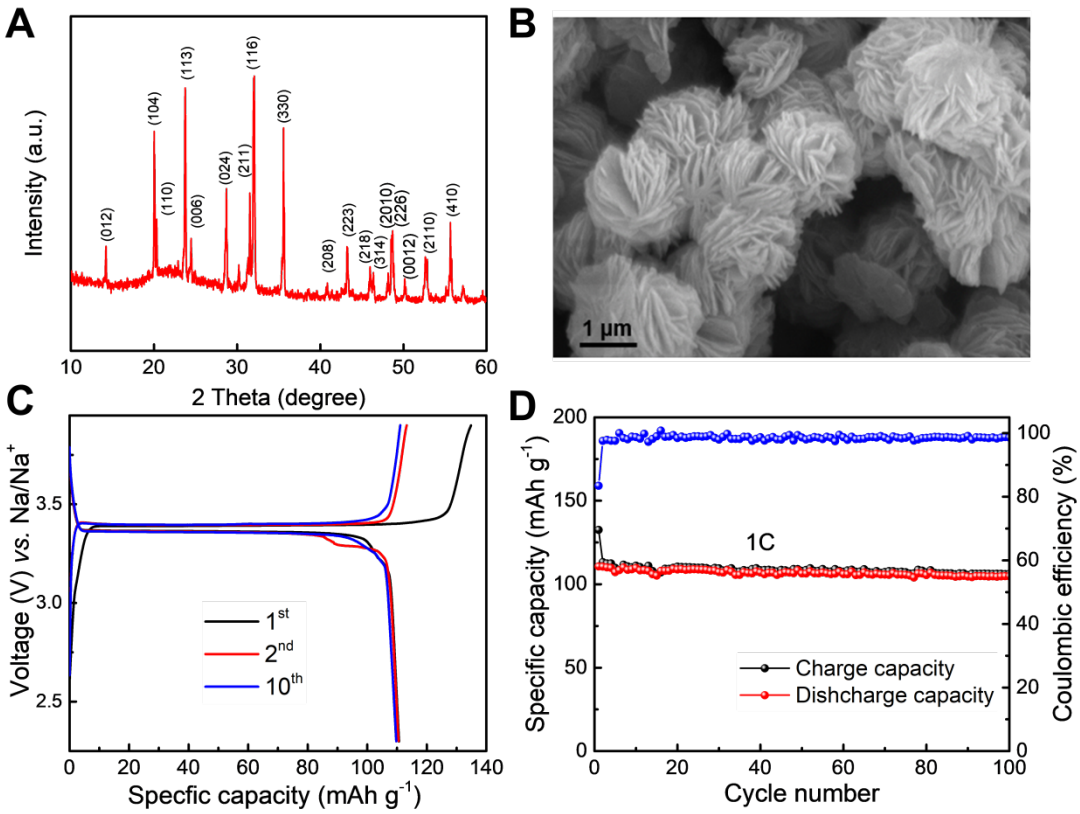

Figure S20. Structural characterizations and electrochemical measurements of $Na_3V_2(PO_4)_3$. (A) XRD and (B) SEM image of $Na_3V_2(PO_4)_3$; (C) Charge and discharge curves of $Na_3V_2(PO_4)_3$ at 1C; (D) Cycling stability and corresponding Coulombic efficiency of $Na_3V_2(PO_4)_3$ at 1C.

Table S1. Morphology comparison of transition metal chalcogenides nanocomposites

Material	Morphology	Loading mode of active material	Ref.
ZnSe@HCNs	Nanoparticles on/in Hollow nanospheres	Outside and inner growth	This work
$CoSe_2$	Urchin-like microflower	bulk	S1
Cu doped $CoSe_2$	Hollow microboxes	Outside growth	S2
$MoSe_2$@HCNs	Nanosheets in hollow nanospheres	Inner growth	S3
FeS_2@C	Yolk-shell nanoboxes	Inner confinement	S4
FeS_2@C	Yolk-shell nanospheres	Inner confinement	S5
ZnS-Sb_2S_3@C	dodecahedron	Inner growth	S6
MoS_2@CMK-3	Nanosheets	Outside growth	S7

Table S2. Tap density calculation of the ZnSe@HCNs and HCNs samples.

Sample	Loading mass /mg	Thickness /um	Diameter /mm	Area /cm^2	Volume /cm^3	Tap density / g cm^{-3}
ZnSe@HCNs	1.35	7.8	12.6	1.25	$9.75*10^{-4}$	1.38
HCNs	1.43	10.6	12.6	1.25	$1.33*10^{-3}$	1.08

Table S3. Electrochemical performance of transition metal selenides anode materials for SIBs

Material	Method	Cyclic stability	Rate performance	Whether possess full battery measurement	Ref.
ZnSe@HCNs	Hydrothermal and calcination	362 mAh g^{-1} at 1 A g^{-1} over 1000 cycles	267 mAh g^{-1} at 20 A g^{-1}	Yes	This work
$NiSe_2$@C	Solvothermal and twice calcination	160 mAh g^{-1} at 3 A g^{-1} over 2000 cycles	241 mAh g^{-1} at 5 A g^{-1}	No	S8
$FeSe_2$	Hydrothermal	372 mAh g^{-1} at 1 A g^{-1} over 2000 cycles	210 mAh g^{-1} at 20 A g^{-1}	Yes	S9
$MoSe_2$/N,P-rGO	Precipitate, hydrothermal and calcination	378 mAh g^{-1} at 0.5 A g^{-1} over 1000 cycles	216 mAh g^{-1} at 15 A g^{-1}	Yes	S10
$SnSe_2$	Hydrothermal	551 mAh g^{-1} at 0.1 A g^{-1} over 100 cycles	221 mAh g^{-1} at 2 A g^{-1}	No	S11
CoSe@C	two hydrothermal and two calcination	299 mAh g^{-1} at 0.1 A g^{-1} over 100 cycles	308 mAh g^{-1} at 5 A g^{-1}	No	S12
Cu doped $CoSe_2$	Hydrothermal and two-step ion-exchange	382 mAh g^{-1} at 1 A g^{-1} over 500 cycles	185 mAh g^{-1} at 3 A g^{-1}	No	S2

Reference

(1) K. Zhang, M. H. Park, L. M. Zhou, G.-H. Lee, W. J. Li, Y.-M. Kang, J. Chen, Adv. Funct. Mater. 26 (2016) 6728-6735.

(2) Y. J. Fang, X. Y. Yu, X. W. Lou, Adv. Mater. 30 (2018) 1706668.

(3) H. Liu, H. Guo, B. H. Liu, M. F. Liang, Z. L. Lv, K. R. Adair, X. L. Sun, Adv. Funct. Mater. 28 (2018)

1707480.

(4) Z. M. Liu, T. C. Lu, T. Song, X. Y. Yu, X. W. Lou, U. Paik, Energy Environ. Sci., 10 (2017) 1576-1580.

(5) Y. X. Wang, J. Yang, S. L. Chou, H. K. Liu, W. X. Zhang, D. Y. Zhao, S. X. Dou, Nature commun., 6 (2015) 8689.

(6) S. H. Dong, C. X. Li, X. L. Ge, Z. Q. Li, X. G. Miao, L. W. Yin, ACS Nano. 11 (2017) 6474-6482.

(7) X. Xu, Z. Y. Fan, X. Y. Yu, S. J. Ding, D. M. Yu, X. W. Lou, Adv. Energy Mater., 4 (2014) 1400902.

(8) X. J. Xu, J. Liu, J. W. Liu, L. Z. Ouyang, R. Z. Hu, H. Wang, L. C. Yang, Min. Zhu, Adv. Funct. Mater., 28 (2018) 1707573.

(9) K. Zhang, Z. Hu, X. Liu, Z. L. Tao, J. Chen, Adv. Mater. 27 (2015) 3305-3309.

(10) F. Niu, J. Yang, N. N. Wang, D. P. Zhang, W. L. Fan, J. Yang, Y. T. Qian, Adv. Funct. Mater. 27 (2017) 1700522.

(11) F. Zhang, C. Xia, J. J. Zhu, B. Ahmed, H. F. Liang, D. B. Velusamy, U. Schwingenschlögl, H. N. Alshareef, Adv. Energy Mater. 6 (2016) 1601188.

(12) C. Wu, Y. Jiang, P. Kopold, P. A. van Aken, J. Maier, Y. Yu, Adv. Mater. 28 (2016) 7276-7283.